Growth patterns in a channel for singular surface energy: Phase-field model

Rahma Guérin and Jean-Marc Debierre
Laboratoire Matériaux et Microélectronique de Provence, Université d'Aix-Marseille III and CNRS, Faculté des Sciences et Techniques de Saint-Jérôme, Case 151, 13397 Marseille Cedex 20, France

Klaus Kassner
Institut für Theoretische Physik, Otto-von-Guericke Universität Magdeburg, Postfach 4120, D-39016 Magdeburg, Germany
(Received 28 July 2004; revised manuscript received 4 November 2004; published 7 January 2005)

We study solidification in a two-dimensional channel for faceted materials whose facets correspond to cusps in the γ plot. The main result is the existence of three growth modes, according to the anisotropy strength: a single faceted finger at high anisotropies, two faceted fingers in the intermediate range, and an oscillating mode at low anisotropies. Simple geometrical and dynamical models are proposed to explain the nature of the observed modes. In particular, the one-finger patterns are shown to be similar to free dendrites while the two-finger patterns correspond to confined solidification fingers.

DOI: 10.1103/PhysRevE.71.011603 PACS number(s): 81.10.Aj, 68.70.+w, 81.30.Fb

I. INTRODUCTION

Owing to its close relationship with two canonical growth models, viscous fingering [1] and dendritic solidification [2], crystal growth in a channel has attracted a rather large interest in the past two decades. The one-sided version of this problem was largely studied by the Green's function method [3–5] and the two-sided version by analytical methods [6,7], numerical resolution of the physical equations [8], and phase-field calculations [9]. The geometrical and physical parameters vary considerably from one paper to the other but a fourfold smooth anisotropy is assumed in each case for the surface energy,

$$\gamma(\theta) = \gamma_0[1 + \epsilon \cos(4\theta)], \tag{1}$$

where θ is the angle between the normal to the interface and the horizontal x axis, perpendicular to the channel axis y.

Analytical results obtained at low Péclet numbers show that two branches of solutions exist for this problem [6]. The low-velocity branch corresponds to the Saffman-Taylor solutions [1], while the high-velocity branch has a different behavior of velocity versus undercooling and describes the solidification fingers. According to the relative strength of two physical parameters, the anisotropy ϵ and channel width W, two regimes are distinguished for the solidification fingers. The geometrical parameter s which gives the zeroth order approximation of the interface equation far from the tip, $y_0 = (1/s)\ln\cos(\pi x/\Delta)$, allows one to discriminate between the two regimes. In the weak anisotropy regime $\pi/\Delta < s < \pi/(1-\Delta)$, confining effects dominate and the selected shape is a confined finger. In the other limit $s < \pi/\Delta$, surface energy dominates, and it crosses over smoothly to the the $W \to \infty$ limit corresponding to a free dendrite.

The purpose of this work is to study the effects of faceting on the growth modes in a channel. Indeed, there exist materials for which the γ plot is not smooth and presents cusps in certain angular directions corresponding to specific crystallographic directions. At equilibrium, facets perpendicular to these directions usually appear.

The growth of dendrites with faceted tips due to cusps in the γ plot was recently studied [10] by the thin phase-field model [11]. The following form of anisotropy was considered:

$$\gamma(\theta) = \gamma_0[1 + \delta(|\sin(\theta - \theta_f)| + |\cos(\theta - \theta_f)|)]. \tag{2}$$

A carefully controlled smoothing of the cusps over a range $\pm\theta_0$ around the facet orientations $\theta_f + n\pi/2$ $(n=0,1,2,3)$ proved necessary to obtain accurate numerical results, which in turn could be extrapolated to the limit $\theta_0 \to 0$.

The present paper deals with the growth of faceted fingers for materials belonging to this family. After a short presentation of the model in Sec. II, we first test it in Sec. III for isotropic surface energy against available results obtained by the Green's function method [5]. We then turn in Sec. IV to the case of anisotropic surface energy for which three growth modes are obtained. Two modes are similar to the ones observed for smooth anisotropy and an oscillating mode is obtained for low anisotropies. A dynamical description of the latter case is proposed in Sec. V, while the former case is analyzed in Sec. VI, within a geometrical model. In Sec. VII, a few points are discussed and additional perspectives opened.

II. PHASE-FIELD MODEL

In the isothermal variational formulation of the thin interface phase-field model [11], the evolution equations for the dimensionless temperature u and phase φ fields are

$$\partial_t u = D\nabla^2 u + \frac{1}{2}\partial_t \varphi \tag{3}$$

and

$$\tau(\theta)\partial_t\varphi = [\varphi - \lambda u(1-\varphi^2)](1-\varphi^2) + \vec{\nabla}[W(\theta)^2\vec{\nabla}\varphi] - \partial_x[W(\theta)W'(\theta)\partial_y\varphi] + \partial_y[W(\theta)W'(\theta)\partial_x\varphi]. \tag{4}$$

In these equations, D is the dimensionless thermal diffusion

coefficient and λ the coupling between temperature and phase fields. The phase field varies continuously across the interface and far from it $\varphi=1(-1)$ in the solid (liquid). The temperature field $u=(T-T_M)/(L_H/C_p)$, with T the temperature, T_M the melting temperature, L_H the latent heat, and C_p the specific heat at constant pressure.

The kinetic coefficient and capillary length are related to the model variables through

$$\beta(\theta) = \frac{a_1}{\lambda}\frac{\tau(\theta)}{W(\theta)}\left[1 - a_2\lambda\frac{W(\theta)^2}{D\tau(\theta)}\right] \tag{5}$$

and

$$d_0(\theta) = \frac{a_1}{\lambda}[W(\theta) + W''(\theta)], \tag{6}$$

where $a_1 \simeq 0.8839$ and $a_2 \simeq 0.6267$ [11] and $\tau(\theta)$ and $W(\theta)$ represent a relaxation time and the interface width.

In this formulation, there is a direct connection between the interfacial energy and the interface width, so that the most natural choice is

$$f(\theta) \equiv W(\theta)/W_0 = \gamma(\theta)/\gamma_0. \tag{7}$$

Here as in [10] the kinetic coefficient is set to zero by imposing

$$\tau(\theta) = \tau_0 f(\theta)^2, \tag{8}$$

so that

$$\lambda = \frac{1}{a_2}\frac{D\tau(\theta)}{W(\theta)^2} = \frac{1}{a_2}\frac{D\tau_0}{W_0^2}. \tag{9}$$

In a small interval $\pm\theta_0$ around the facet orientations, the anisotropy function is smoothed; for instance one uses

$$f(\theta) = 1 + \delta/\sin\theta_0 + \delta(1 - \cot\theta_0)\cos(\theta - \theta_f) \tag{10}$$

in the range $0 \leqslant \theta - \theta_f \leqslant \theta_0$ [10]. The discretization of the model is based on a simple Euler scheme on a regular square mesh and is described at length in Ref. [10]. We impose a mesh size $h/W_0=0.4$ and a diffusion coefficient $D\tau_0/W_0^2 = 1.0$ throughout the paper. The domain considered is the channel $-L \leqslant x \leqslant L$ and $-H \leqslant y \leqslant H$, with $L/W_0=37.6$ and $H/W_0=100.0$, 200.0, or 400.0. We only consider the facet orientation $\theta_f=\pi/4$ here. Other orientations are possible but symmetry about the growth direction, i.e., the y axis, is broken then. This introduces an additional degree of freedom in the problem and, in the case of smooth anisotropy, it was shown that the resulting competition between growth and channel orientations gives rise to additional dynamical modes as periodically oscillating structures [12]. The specific choice $\theta_0=K\delta/(1+\delta)$ for the smoothing angle permits us to use a time step that is independent of δ. In the simulations we impose $K=\pi/25$, so that $\delta t/\tau_0=0.032$; this rather large time step brings the computation times down to practical values.

Throughout the present paper we will systematically use nondimensional variables, lengths $\tilde{x}=x/(2L)$ and times $\tilde{t}=t/(4L^2/D)$, so that nondimensional velocities $\tilde{V}=V \times (2L/D)$ are in fact, up to a constant factor, Péclet numbers.

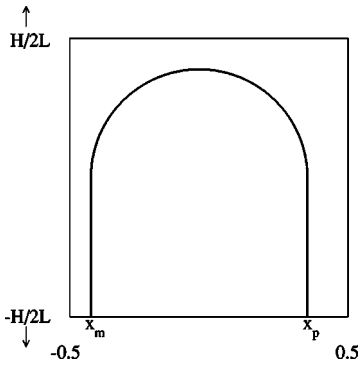

FIG. 1. Shape of the germ used as initial condition in the phase-field simulations.

In the following, the tildes will be dropped in order to simplify the notation. Unless otherwise stated, the same reduced capillary length $d_0/(2L)=0.005$ as in Ref. [5] will be used.

III. RESULTS FOR ISOTROPIC SURFACE ENERGY

We first test our code by considering the case of isotropic surface energy, i.e., $\delta=0$. The initial condition is a solid finger ($\varphi=1$) with the shape of a rectangle $x_m \leqslant x \leqslant x_p$ and $-H/2L \leqslant y \leqslant 0$, topped by a half circle and with the width expected in the stationary state, $x_p - x_m = \Delta$ (see Fig. 1). A horizontal shift is imposed ($x_p \neq -x_m$) in order to promote the development of asymmetric fingers whenever they are stable. The temperature field u is initially set to zero inside the solid germ and to $-\Delta$ outside. Reflecting conditions are imposed at all the domain boundaries. In order to keep the tip at a roughly constant altitude during the whole simulation length, the phase and temperature fields are shifted downward at regular time intervals. The area freed at the top of the domain is then filled with pure liquid ($\varphi=-1$) at temperature $u=-\Delta$.

After a transient which shortens as undercooling is increased, the finger reaches a stationary state in which its tip moves at a constant velocity V.

Tip velocity is plotted as a function of undercooling in Fig. 2. Our data agree qualitatively well with the corresponding results obtained by Kupferman *et al.* [5]. The obvious quantitative differences are not unexpected since these authors studied the one-sided version of the problem, whereas our model describes the two-sided case.

At low undercoolings, $\Delta < 0.73$, symmetric fingers are obtained, while parity broken fingers are selected for $\Delta > 0.73$. For $\Delta=0.73$, an asymmetric finger arises from the off-centered initial condition. However, using the stationary symmetric finger obtained for $\Delta=0.72$ as initial condition, we also obtain a stable symmetric finger for $\Delta=0.73$. As expected, the asymmetric finger grows faster. The bifurcation point lies near $\Delta_B \simeq 0.725$ which is significantly higher than the value $\Delta_B \simeq 0.665$ obtained in [5].

Below some critical value $\Delta^*(0) \simeq 0.68$, the initial finger is systematically unstable and the interface evolves slowly to a planar front.

IV. RESULTS FOR ANISOTROPIC SURFACE ENERGY

We now turn to the main purpose of this paper, which is the growth of materials with cusps in the γ plot. We set the

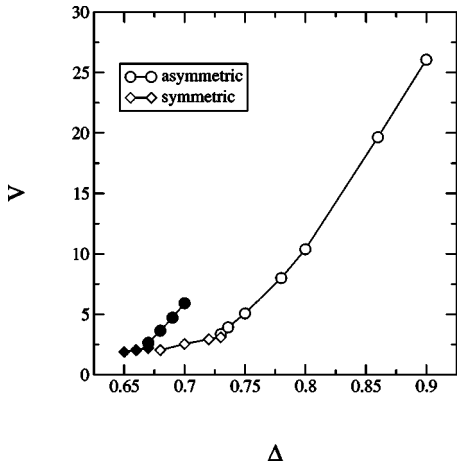

FIG. 2. Tip velocity as a function of undercooling for isotropic surface energy (open symbols). Note the coexistence of the symmetric and asymmetric modes for $\Delta=0.73$. The corresponding data of Kupferman *et al.* are also shown for comparison (filled symbols).

undercooling to a fixed value, $\Delta=0.78$, high enough for the simulation times to be reachable.

The only free parameter is thus the anisotropy strength δ and Fig. 3 represents the tip velocity as a function of this parameter. We use both centered and off-centered initial conditions here; as a consequence, two dynamical modes may coexist for some values of the anistropy strength δ. Anisotropy favors growth since the tip velocity $V(\delta)$ for $\delta>0$ is systematically higher than $V(0)$.

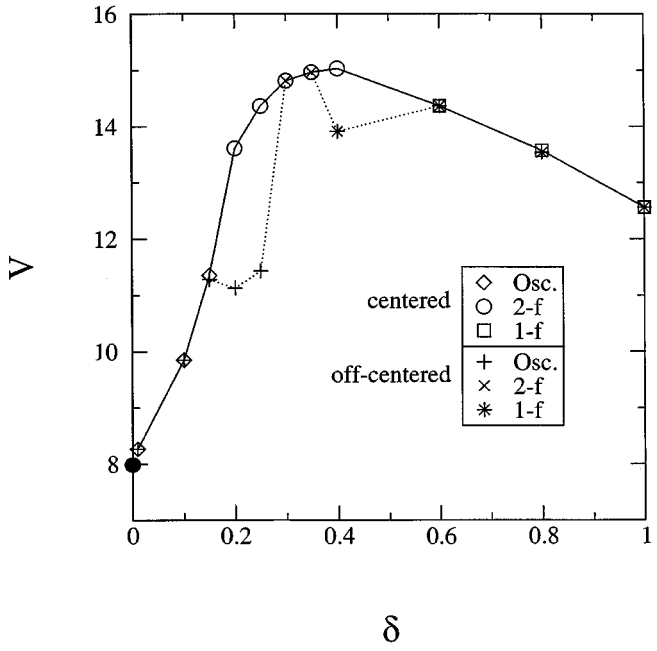

FIG. 3. Morphology diagram for anisotropic surface energy. Tip velocity is plotted as a function of anisotropy for centered and off-centered initial conditions. The black circle corresponds to the asymmetric finger obtained at zero anisotropy.

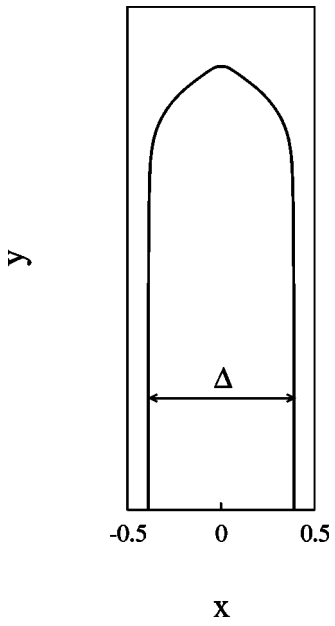

FIG. 4. One faceted finger obtained for undercooling $\Delta=0.78$ and anisotropy $\delta=1.0$. The x and y coordinates are normalized by the total channel width.

A. High anisotropy: One faceted finger

For $\delta\geqslant 0.6$, a single faceted finger is obtained independently of the initial condition, as shown in Fig. 4.

An important prerequisite is to check numerical convergence of the finger shape as the rounding angle θ_0 tends to zero. In Fig. 5 the facet length Λ and the tip radius R are plotted as functions of θ_0. A satisfactory linear convergence is observed, as in the case of dendritic growth [10]. Note that, because of the rather long times needed to perform the numerical simulations, we do not extrapolate our data to the limit $\theta_0\rightarrow 0$ in the following. Based on the results obtained here, one can expect systematic deviations of less than 20% on Λ and R.

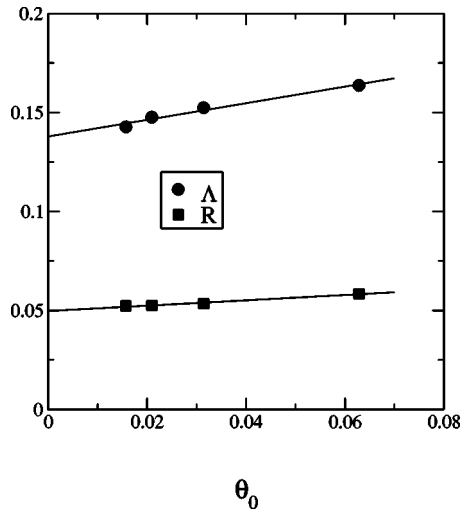

FIG. 5. Convergence of the tip radius R and facet length Λ with the rounding angle θ_0 (anisotropy $\delta=1.0$).

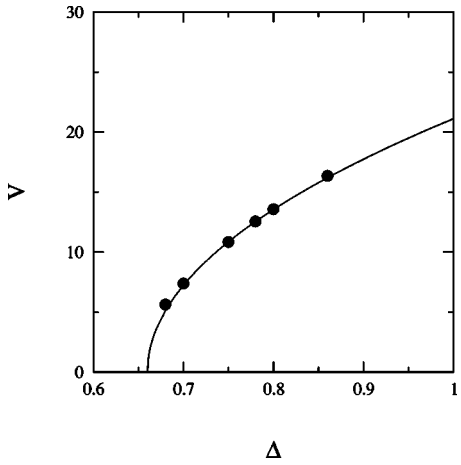

FIG. 6. Tip velocity as a function of undercooling for the one-finger mode and constant anisotropy, $\delta=1.0$. The continuous line is a least-squares fit to a square-root law.

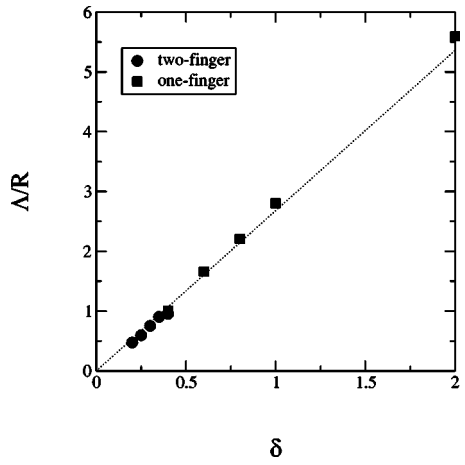

FIG. 8. Ratio of the facet length to the tip radius as a function of anisotropy for the one- and two-finger modes. The straight dotted line is a guide to the eye.

Contrary to the isotropic case ($\delta=0$), the finger is always symmetric in this range of anisotropy. This is not so surprising because higher surface energy anisotropy imposes higher symmetry about the y axis. This result is not due to a particular choice of undercooling, since keeping the anisotropy fixed at $\delta=1.0$ and varying Δ, we systematically obtain one symmetric faceted finger for $\Delta \geqslant 0.68$. On the other hand, we cannot totally exclude the existence of a stability domain for asymmetric faceted fingers in the (δ,Δ) plane.

Tip velocity is plotted as a function of undercooling in Fig. 6 for an anisotropy $\delta=1$. The data follow reasonably well the law $\Delta=\Delta^*+aV^2$ $(a>0)$ valid for supercritical bifurcations. To check the possibility of a subcritical bifurcation, we also try a fit of the form $\Delta=\Delta^*+aV^2+bV^4$, which, however, yields a negative b value, essentially excluding a subcritical bifurcation. A least-squares fit to the first law then gives $\Delta^*(1)\simeq 0.66$ for the critical undercooling, to be compared to $\Delta^*(0)\simeq 0.68$ obtained for zero anisotropy. A decrease of the critical undercooling $\Delta^*(\delta)$ on anisotropy increase is also found for the usual $\cos 4\theta$ anisotropy term [5].

B. Intermediate anisotropy: Pair of faceted fingers

A pair of faceted fingers is spontaneously selected when $0.20 \leqslant \delta \leqslant 0.40$ for centered initial condition and when $0.30 \leqslant \delta \leqslant 0.35$ for off-centered initial condition (Fig. 7). This mode is the fastest one in the present study (see Fig. 3).

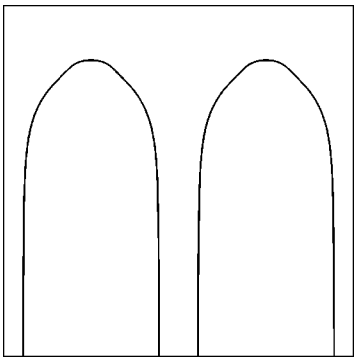

FIG. 7. A pair of faceted fingers obtained for undercooling $\Delta=0.78$ and anisotropy $\delta=0.30$.

In Fig. 8, Λ/R is plotted as a function of the anisotopy stength δ for the one-finger and the two-finger modes. Linear increase is observed in both cases, and the transition, between the two modes occurs for $\delta=0.40$, where $\Lambda/R\simeq 1$. Insight into the origin of this transition is provided by the analytical study of the smooth anisotropy case [6]. For strong anisotropy, the finger dynamics is governed by surface energy and is thus similar to that of a free dendrite. On the other hand, for weak anisotropy, confining effects are dominant and a different shape is selected. This picture is tested quantitatively for faceted solidification in the framework of a geometrical model in Sec. VI.

At this point, it is rather instructive to compare the two-finger mode (Fig. 7) with the dendritic pattern obtained in the open space for the same parameters (Fig. 9). The latter also displays two main parallel branches but their overall width exceeds the channel width by far. In addition it is clearly visible on the figure that the widths of these branches are constantly increasing, which should cause new tip splittings at later times (we indeed observe late tip splittings when starting from a different germ). This dendritic pattern is thus essentially nonstationary, contrary to the stationary two-finger pattern obtained in the channel. The velocity of the highest dendrite tip is represented as a function of time in Fig. 10. It is evident from this plot that it would take an extremely long time for the system to reach a stationary state, if ever. We also see from this figure that the dynamics is quite sensitive to the initial condition. In any case, the velocity seems to adopt as an upper bound the stationary velocity of the two-finger mode. This observation clearly suggests that confining due to the channel walls allows the system to select a fast stationary state that is probably not reachable in an open geometry.

The stability of such patterns may be questioned because periodic arrays of fingers are not observed during solidification in an open space. This question is especially relevant when another dynamical state is obtained for a different initial condition, like the one-finger mode at $\delta=0.40$ or the

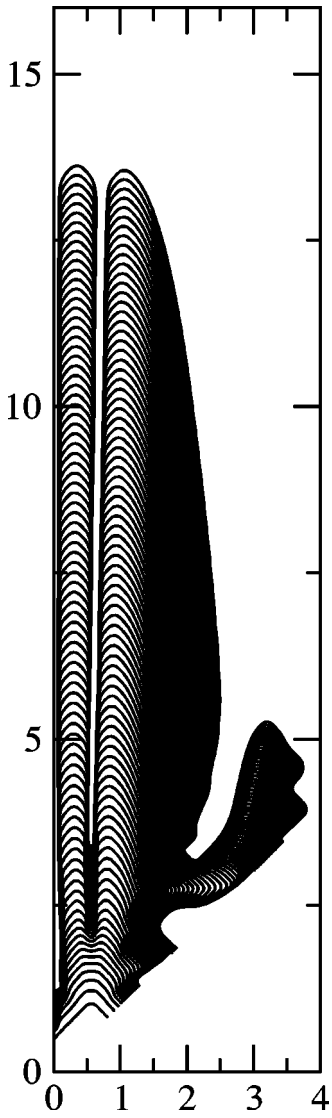

FIG. 9. A dendritic pattern obtained with the same parameters as the two fingers shown in Fig. 7.

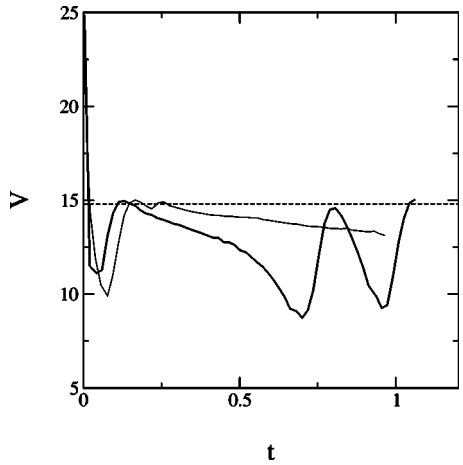

FIG. 10. Time evolution of the velocity for the highest tip of the dendritic pattern shown in Fig. 9 (thick line). The thin line corresponds to a different initial condition (solid germ). The horizontal dashed line gives the velocity selected by the two-finger mode in the channel geometry.

oscillatory mode described in the next section at $\delta=0.20$ and $\delta=0.25$. In order to check the stability of the two-finger patterns, we introduce a small perturbation (a square dip) at the tip of one of the two fingers and resume time evolution. On the large anisotropy side ($\delta=0.40$), we indeed observe that the perturbed finger is eliminated at long times and we recover the one-finger mode obtained for off-centered initial conditions. On the small anisotropy side, ($\delta=0.20$) the perturbation again provokes finger elimination and leads to the final oscillatory mode obtained with an off-centered initial condition. Both cases confirm that the two-finger mode may be dynamically unstable. However, the two-finger pattern obtained for $\delta=0.25$ does remain stable against tip perturbation. Since this mode is also obtained both from centered and off-centered initial conditions for $\delta=0.30$ and $\delta=0.35$, we conclude that there should exist a narrow stability domain for the two-finger mode. The stability domain probably gets narrower for higher order periodic patterns (three, four, etc., fingers) because more total space is available then for rearranging the structures. This would explain why they are not observed in open space.

C. Low anisotropy: Oscillatory mode

For $\delta\leqslant 0.25$, oscillatory states with a very stable period T are observed at long times, the same state being reached from both centered and off-centered initial conditions (Fig. 11).

To understand this mode, let us remark that growth always starts with tip splitting of the initial germ. Competition between the two resulting fingers increases as anisotropy is decreased because facets become shorter, so that geometrical constraints are weaker. In this competition, one finger is ultimately eliminated and the survivor tries to adopt an asymmetric shape as for zero anisotropy. On the other hand, surface stiffness tends to maintain symmetry about the y axis. Competition between both effects results in a new tip splitting and leads to the observed oscillations. In the case of centered initial condition, the initial tip splitting preserves symmetry about the y axis so that the double-finger mode remains stable for high enough anisotropies ($\delta=0.20$ and $\delta=0.25$).

The tip of the main finger is defined as the highest point of the interface, $M(x,y)$, and its vertical velocity is denoted V_y. Following the tip trajectory together with the evolution of the whole pattern gives valuable informations about the oscillating mode (see Fig. 11). For off-centered initial conditions, M remains on the right of the channel and slightly oscillates around an average abscissa $\langle x\rangle$. Let us choose the time origin as the moment when M passes through its average x position $x(0)=\langle x\rangle$ while moving to the right. At $t=0$, a shoulder appears on the main finger, on the left side of the tip. This shoulder is the precursor of a secondary finger $S(x',y')$, which is created after about an eighth of a period, $t\simeq T/8$, at abscissa $x'(T/8)\simeq 0$. Note that right from the start the secondary finger is lower than the main one $y'(T/8)$

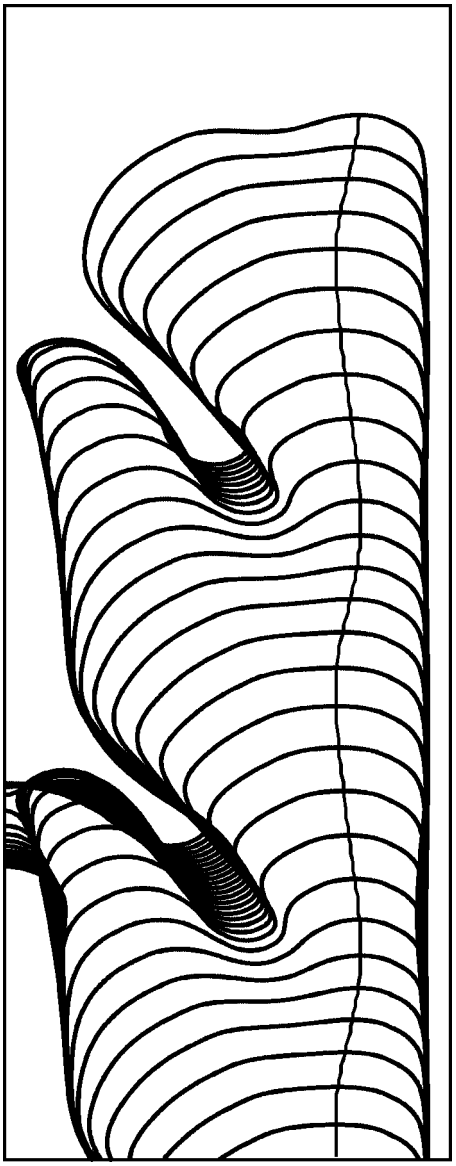

FIG. 11. Oscillating mode obtained at undercooling $\Delta=0.78$ for anisotropy $\delta=0.10$. The trajectory of the main finger tip M is superimposed on the interface contours.

$<y(T/8)$, and that $y-y'$ increases steadily in time. Initially the two fingers repel each other, M moving to the right and S to the left. Tip splitting provokes a vertical acceleration of M, so that V_y starts to increase at time $t=T/8$. At time $t \simeq T/4$, the main finger rebounds on the right channel wall and M starts to move leftward. Meanwhile, the tip velocity continues to increase to reach a maximum at time $t \simeq 4T/10$, when M passes again through its average position, $x=\langle x\rangle$. The leftward movement of the main finger stops when it bounces on the secondary finger at time $t=8T/10$ and M backtracks again. During the remaining time interval $8T/10 \leqslant t \leqslant T$, the main tip M moves again to the right while V_y continues to decrease. Finally, at $t=T$ the secondary finger S stops growing vertically (elimination) and then rapidly spreads sideways to reach the left channel wall. The system is now ready for the next cycle. From this analysis, one sees that the vertical velocity V_y oscillates around an average

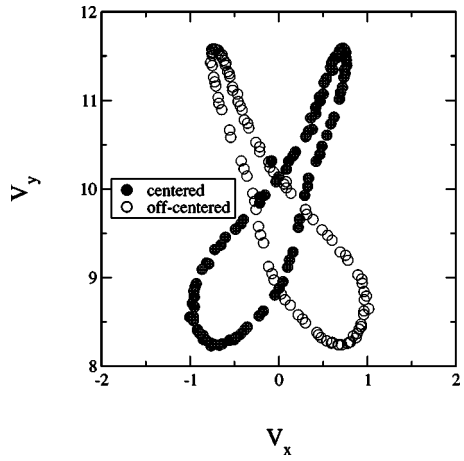

FIG. 12. (V_x, V_y) plots obtained with two different initial conditions for the oscillating mode displayed in Fig. 11.

value V. Since V_y increases (decreases) for about 40% (60%) of the period T, these oscillations are far from being sinusoidal. The same is true for the horizontal component of the tip velocity V_x which oscillates around zero.

The (V_x, V_y) plot displays the limit cycle corresponding to the oscillating mode (Fig. 12). Depending on the transient, either the rightmost or the leftmost finger may be repeatedly eliminated. For this reason two symmetric cycles are obtained for centered and off-centered initial conditions. We obtain qualitatively similar (V_x, V_y) cycles for all the low anisotropies considered here but details in the dynamics can be somewhat different. For instance, for $\delta=0.20$ and 0.25 the secondary finger stops its growth on the right wall and the left wall alternately.

V. DYNAMICAL MODEL FOR THE OSCILLATING FINGERS

An attempt to model the cyclic motion engendered by repeated tip splitting and elimination of one finger faces the primary difficulty that if we choose geometric variables describing the positions of features of the fingers, the loss of a finger also means the loss of periodicity, since the newly created finger is not identical with the old one. For example, we would like to choose the difference of the coordinates of two finger tips as dynamical variables, because an interaction between the two fingers will predominantly depend on their distances in the two coordinate directions. But these distances become undefined as soon as one of the fingers disappears and a new set of distances arises as a finger is created. To circumvent this difficulty, we concentrate on variables describing a single finger and use plausible assumptions together with symmetry considerations to construct a phenomenological model that should capture the essential aspects of the interaction between fingers.

Our first assumption is that inertial effects do not play any role in the slow finger dynamics. This means that we will not write equations for accelerations of the finger but rather consider the overdamped limit in which only velocity terms and coordinates appear. An obvious advantage is that we will

have just two first-order equations of motion for the tip position (i.e., the x and y coordinates of a finger) instead of two second-order ones.

Next we note that there are four distinguished directions in the system. Two are the y and x directions, determined by the walls of the channel and the direction orthogonal to them. The other two are the directions of the facets which are oriented at an angle of 45 degrees with respect to the x and y directions. These orientations can be described by equations of the form $x+y=\text{const}$ and $x-y=\text{const}$. So our model should be written in terms of the variables x, y, $x-y$, and $x+y$ (which are not independent of each other, of course).

Third, we require all nonlinear terms in the model equations to respect the basic symmetry under reflection ($x \rightarrow -x$) with respect to the axis of a finger (in the case of a two-finger solution $x=0$ corresponds to a coordinate that is off center by a quarter of the channel width). We do not require the same thing for the linear terms. These terms will drive the bifurcation from a fixed tip position (in the frame moving with the average tip velocity) to an oscillating tip. One might, for example, assume that the linear terms contain the control parameter as a common prefactor. This bifurcation parameter crosses the value zero at the bifurcation point, where the linear terms are therefore absent and the required symmetries of the system are respected. Beyond the bifurcation, the symmetry would be broken by the fact that either the left or the right finger is the one that survives, and this symmetry breaking is reflected by a symmetry breaking in the linear terms of the model. On the other hand, if the bifurcation is of true Hopf type, i.e., if the oscillations start with a finite frequency, then not all linear terms in the model equations (11) and (12) given below would have vanishing coefficients at the bifurcation point. But this would not be a problem either, because the *total* system need not be symmetric with respect to $x=0$ but only with respect to the channel center. Only the fingers themselves and the diffusion field in the vicinity of their tips will satisfy the discussed symmetry (approximately). In the case of a Hopf bifurcation, one finger would correspond to one set of parameters of the linear terms, the other to the symmetric set, as will be discussed shortly.

If we restrict ourselves to nonlinearities up to third order, we may then write a simplified model as follows:

$$\dot{x} = a_1 x + b_1 y - x\left[\left(\frac{x-y}{c}\right)^2 + \left(\frac{x+y}{c}\right)^2\right] + exy \qquad (11)$$

and

$$\dot{y} = -b_2 x + a_2 y - y\left[\left(\frac{x-y}{d}\right)^2 + \left(\frac{x+y}{d}\right)^2\right]. \qquad (12)$$

Further terms allowed by symmetry would be additional terms proportional to x^3 and xy^2 in the first equation and terms proportional to y^2 and y^3 in the second. However, we will not invoke these terms here in order not to proliferate parameters unnecessarily. That the prefactors of the $x-y$ and $x+y$ terms are the same in each equation is a consequence of our symmetry requirements for the nonlinear terms. The symmetry-breaking terms are the terms with the coefficients b_1 and b_2. For each solution of this phenomenological model there is a symmetric partner obtained after replacing $b_1 \rightarrow -b_1$ and $b_2 \rightarrow -b_2$, corresponding to the other finger being the survivor of the competition.

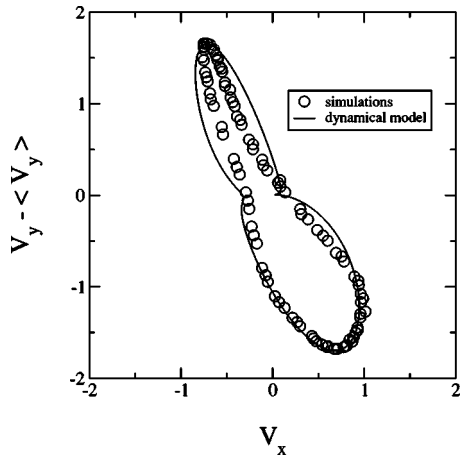

FIG. 13. Comparison of the numerically determined tip velocity with that obtained from the model equations (11) and (12), with parameter values $a_1=0.6$, $a_2=0.45$, $b_1=0.245$, $b_2=0.8$, $c=6.35$, $d=3.84$, and $e=0.04$. The parameters were fitted by eye.

The linearized problem arising from Eqs. (11) and (12) has the eigenvalues

$$\lambda_{1/2} = \frac{1}{2}(a_1 + a_2) \pm \sqrt{\frac{1}{4}(a_1 - a_2)^2 - b_1 b_2}.$$

Negative values of a_1 and a_2 (or a negative sum) produce a fixed point $x=y=0$, and we expect the model to describe oscillating tips for a range of positive values of all parameters.

A physical interpretation of the terms in this model is as follows. The parameters a_1 and a_2 trigger the oscillatory instability, so they must increase with decreasing anisotropy. Whether b_1 or b_2 is roughly constant at the bifurcation or crosses zero depends on whether the bifurcation is a Hopf bifurcation or not, i.e., on whether the oscillations start at a finite frequency or at zero frequency. Our data support the first possibility. The terms containing $x-y$ and $x+y$ describe the influence of the facets. They contain length scales c and d which must be formed from the length scales of the physical problem, that is, the diffusion length, the capillary length, and the length of the facets. Since these terms should vanish in the absence of facets, c and d must increase with decreasing facet length. An inverse proportionality would therefore be a possible relationship. c and d need not be equal, since the x and y directions are not equivalent. The term proportional to xy is present, because growth in the x and y directions is coupled even in the absence of facets, and this is the simplest term describing such a coupling. Note, however, that in the absence of anisotropy and, hence, facets, the model as it stands cannot describe instability of a steady finger. We would then have to take into account at least the cubic terms that were neglected above ($\propto x^3$ and $\propto y^3$).

In Fig. 13, we show a comparison of the numerically observed tip velocity for an undercooling of 0.78 and an aniso-

tropy strength of 0.10 with the model. In order to do the comparison, the average tip position has to be subtracted out to move the fixed point of the numerical finger to $y=0$.

As the figure demonstrates, a quite reasonable agreement can be obtained, which suggests that the ingredients contributing to the oscillatory motion are indeed the ones mentioned (the competing effect of the four principal directions together with a destabilization of the steady tip by the driving force of the growth, restricted by the system symmetries). It should also be noted that the model is quite sensitive to some of its parameters (b_1, for example, but also c and d), small changes of which will lead to the system collapsing into a new fixed point. This agrees well with the numerical observation that oscillations exist only in a limited parameter range and disappear again as anisotropy goes to zero.

In fact, the simulations show that if, starting from an oscillating system, we increase the anisotropy, the system moves toward a steady solution consisting of two fingers. This parameter change in the numerics corresponds to a reduction of the parameters a_1, a_2, c, and d, which leads to the fixed point $x=y=0$ corresponding to the two-finger solution, as soon as the sum of a_1 and a_2 falls below zero. On the other hand, a decrease of the anisotropy to zero leads back to a steady single-finger solution in the numerics, and an increase of c and d normally leads to a fixed point different from $x=y=0$ in the model, which it should, because the steady single finger is positioned at $x=L/4$ or $x=-L/4$ in the model. That the model is quantitative well beyond the bifurcation should not be expected, but it seems to give the right qualitative answers.

VI. GEOMETRICAL MODEL FOR THE FACETED FINGERS

At high and intermediate anisotropies, symmetric faceted fingers are selected. A close examination of the fingers obtained in the numerical simulations suggests splitting the function $y(x)$ that describes the interface into three sectors (Fig. 4).

(1) Circular tip of radius R,

$$y = y_0 - R + (R^2 - x^2)^{1/2}, \quad 0 \leqslant x \leqslant x_1. \tag{13}$$

(2) Linear facet of length Λ,

$$y = y_1 - (x - x_1), \quad x_1 \leqslant x \leqslant x_2. \tag{14}$$

(3) Trailing part asymptoting a vertical line,

$$y = \frac{1}{s} \ln \cos\left(\frac{\pi x}{\Delta}\right), \quad x \geqslant x_2. \tag{15}$$

In the above equations, we restrict ourselves to the half plane $x \geqslant 0$ (symmetric finger) and we use the notations $x_1 = R/\sqrt{2}$, $x_2 = (R+\Lambda)/\sqrt{2}$, $y_0 = y(0)$, and $y_1 = y(x_1)$.

Sectors 1 and 2 describe the tip of the faceted finger which is similar to one of the four rounded corners present in the equilibrium shape [10,13,14]. In sector 3, the interface is almost vertical and the anisotropy term is thus practically constant. The zeroth approximation of the finger shape [Eq. (15)] proposed in Ref. [6] for smooth anisotropy is thus also valid here. In this approximation, there exists an implicit relation between the geometrical parameter s and the Péclet number

$$p = V/(2n_f), \tag{16}$$

where n_f is the number of fingers growing simultaneously [6]. This relation reads

$$d_0 s\{\tan(\Delta a) + \tan[(1-\Delta)a]\} = p/a, \tag{17}$$

where

$$a = \frac{1}{2}[s(s+2p)]^{1/2}. \tag{18}$$

Expressing the continuity of $y(x)$ and $y'(x)$ at $x=x_1$ and $x=x_2$ allows one to obtain all the geometrical parameters but one (x_1) as functions of s. Once a value is provided for x_1, the interface equation $y(x)$ is completely determined and one can compute the temperature field everywhere along the interface by using the boundary integral expression

$$u(x) = -\Delta + p \sum_{n=-\infty}^{n=+\infty} \int_{-\Delta/2}^{+\Delta/2} \frac{dx'}{\pi} \exp(-p[y(x) - y(x')]) \times K_0(p\sqrt{(x - x' + n)^2 + [y(x) - y(x')]^2}), \tag{19}$$

where K_0 is the zeroth order modified Bessel function. Two additional equations are still available to complete our geometrical model [10]. One is the Gibbs-Thomson relation expressed at the finger tip,

$$u(0) = -d_0/R, \tag{20}$$

and the other relates the average undercooling on the facet to the cusp amplitude,

$$\delta = \frac{1}{\sqrt{2}u(0)R} \int_{R/\sqrt{2}}^{(R+\Lambda)/\sqrt{2}} dx\, u(x). \tag{21}$$

The algorithm implemented to solve the present geometrical model is the following.

(a) Fix the geometrical parameter s.

(b) Compute the Péclet number p from Eqs. (17) and (18).

(c) Set the tip radius R to a reasonable guess.

(d) Compute the temperature at the finger tip, $u(0)$, from Eq. (19) and deduce a new estimate of R from Eq. (20). Repeat this step until convergence on R.

(e) Use Eq. (21) to compute the anisotropy strength δ.

As stated previously, the two-finger mode ($n_f=2$) obtained at lower anisotropies is expected to fall in the weak anisotropy regime [6]. This regime corresponds to a simple condition on the geometrical parameter s,

$$\pi/\Delta < s < \pi/(1-\Delta). \tag{22}$$

In the geometrical model, we have

$$x_2 = n_f\left(\frac{\Lambda + R}{\sqrt{2}}\right) = \frac{\Delta}{\pi} \tan^{-1}\left(\frac{\Delta s}{\pi}\right). \tag{23}$$

Using our numerical values of R and Λ, we verify that s indeed satisfies the conditions prescribed by Eq. (22).

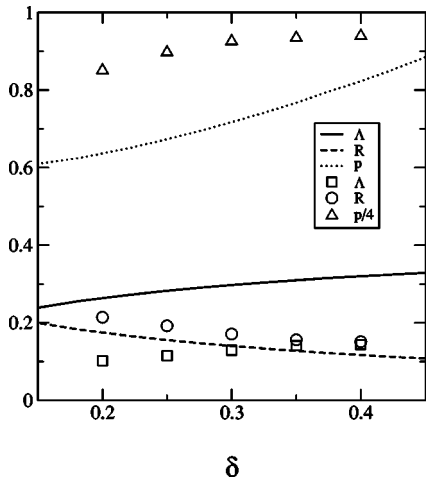

FIG. 14. Comparison of the finger features obtained in the geometrical model (lines) and in the numerical simulations (symbols) for the two-finger mode. Note the two different scales for the Péclet number p.

Figure 14 displays the variations of the tip parameters Λ and R and Péclet number p as functions of anistropy δ for the two-finger mode. The agreement between the geometrical model and the numerical data is qualitatively good: the variations of the three parameters follow the same trends in both cases. Quantitative agreement cannot be expected, however, since the model developped in Ref. [6] is for small Péclet numbers while the Péclet numbers obtained in the simulations are rather large.

On the other hand, the geometrical model fails to predict the results obtained for the one-finger mode, at higher anisotropies. For instance, it predicts that the velocity should increase on anisotropy increase, contrary to what is found in the simulations (see Fig. 3). This is not surprising because we find that $s < \pi/\Delta$ for high anisotropies. This corresponds to the strong anistropy limit of Ref. [6], i.e., to the dendritic regime. To test this point, we simulated the growth of a free dendrite for anisotropy $\delta = 1.0$, using the same physical and phase-field parameters as in the channel. The operating state parameters of the dendrite are given in Table I, together with their counterparts for the one-finger mode obtained in the channel geometry. These results clearly confirm that our one-finger mode belongs to the dendritic branch of solutions.

TABLE I. Comparison of the normalized facet length, tip radius, and Péclet number between a finger and a dendrite grown with the same parameters (undercooling $\Delta = 0.78$, anisotropy $\delta = 1.0$).

Λ	R	p	
0.171	0.059	6.30	Dendrite
0.164	0.058	6.27	Finger

VII. CONCLUSIONS

The main outcome of this paper about solidification in a channel is to reveal a number of similarities as well as clear differences between rough and faceted materials. For deep enough cusps in the surface free energy, the faceted fingers either behave like free faceted dendrites or adopt a faster growth mode corresponding to the confined finger. These two modes are qualitatively comparable to the ones found for smooth anisotropy in the surface energy [6].

On the other hand, for shallow cusps an oscillating mode is found that, to our knowledge, has no counterpart for rough materials. This mode is obtained in a rather wide domain of anisotropies, $0.01 \leqslant \delta \leqslant 0.25$, but we only consider one specific combination of the two other physical parameters, undercooling and capillary length here. A systematic study of the stability domain of this mode would be desirable.

Alternatively, we do not observe faceted asymmetric fingers in the present study, and the domain of existence of this mode should be sought for more systematically than by varying the undercooling alone, as we do here.

A careful look at the oscillating mode reveals that the main finger is rather similar in shape to the nonfaceted asymmetric finger obtained at zero anisotropy. Moreover, there is no discontinuity in the average vertical growth rate as anisotropy tends to zero (see Fig. 3). This suggests that the oscillating and the asymmetric modes are closely related. In fact, our numerical results indicate a continuous transition from the oscillating mode to the steady asymmetric finger as anisotropy is decreased to zero: the relative amplitude of the oscillations progressively vanishes while the growth patterns look more and more like the asymmetric finger.

[1] P. G. Saffman and G. I. Taylor, Proc. R. Soc. London, Ser. A **245**, 312 (1958).
[2] For a review, see, e.g., E. A. Brener and V. I. Mel'nikov, Adv. Phys. **40**, 53 (1991).
[3] D. A. Kessler, J. Koplik, and H. Levine, Phys. Rev. A **34**, 4980 (1986).
[4] E. Brener, H. Müller-Krumbhaar, Y. Saito, and D. Temkin, Phys. Rev. E **47**, 1151 (1993).
[5] R. Kupferman, D. A. Kessler, and E. Ben-Jacob, Physica A **213**, 451 (1995).
[6] E. A. Brener, M. B. Geĭlickman, and D. Temkin, Sov. Phys. JETP **67**, 1002 (1988).
[7] M. Ben Amar and E. Brener, Phys. Rev. Lett. **75**, 561 (1995).
[8] T. Ihle and H. Müller-Krumbhaar, Phys. Rev. E **49**, 2972 (1994).
[9] F. Marinozzi, M. Conti, and U. M. Marconi, Phys. Rev. E **53**, 5039 (1996).
[10] J. M. Debierre, A. Karma, F. Celestini, and R. Guérin, Phys. Rev. E **68**, 041604 (2003).
[11] A. Karma and W. J. Rappel, Phys. Rev. E **53**, R3017 (1996); **57**, 4323 (1998).
[12] H. Emmerich, D. Schleussner, T. Ihle, and K. Kassner, J. Phys.: Condens. Matter **11**, 8981 (1999).
[13] M. Adda Bedia and V. Hakim, J. Phys. I **4**, 383 (1994).
[14] M. Adda Bedia and M. Ben Amar, Phys. Rev. E **51**, 1268 (1995).